Hoyle-analog state in ^{13}C studied with antisymmetrized molecular dynamics

Y. Chiba

Department of Physics, Hokkaido University, 060-0810 Sapporo, Japan
and Research Center for Nuclear Physics (RCNP), Osaka University, Ibaraki 567-0047, Japan

M. Kimura

Department of Physics, Hokkaido University, 060-0810 Sapporo, Japan;
Nuclear Reaction Data Centre, Faculty of Science, Hokkaido University, Sapporo 060-0810, Japan;
and Research Center for Nuclear Physics (RCNP), Osaka University, Ibaraki 567-0047, Japan

The cluster states in ^{13}C are investigated by antisymmetrized molecular dynamics. By investigating the spectroscopic factors, the cluster configurations of the excited states are discussed. It is found that the $1/2_2^+$ state is dominantly composed of the ^{12}C(0_2^+) $\otimes s_{1/2}$ configuration and can be regarded as a Hoyle-analog state. On the other hand, the p-wave states ($3/2^-$ and $1/2^-$) do not have such structure, because of the coupling with other configurations. The isoscalar monopole and dipole transition strengths from the ground to the excited states are also studied. It is shown that the excited $1/2^-$ states have strong isoscalar monopole transition strengths consistent with the observation. On the other hand, the excited $1/2^+$ states unexpectedly have weak isoscalar dipole transitions except for the $1/2_1^+$ state. It is discussed that the suppression of the dipole transition is attributed to the property of the dipole operator.

I. INTRODUCTION

Currently, the Hoyle state of ^{12}C [1–6] attracts much interest as a possible bosonic condensate. A natural extension of this interest is the search for the analog states in heavier $4n$ nuclei such as ^{16}O and ^{20}Ne. Recently, a possible candidate in ^{16}O [7–10] has been intensively discussed, and a theoretical study [11] predicted the existence of the α particle condensate up to approximately the 10α system ^{40}Ca.

Another direction of the research is the study of $N \neq Z$ nuclei in which nucleon particles or holes can be injected into the α particle condensate as an impurity. In the case of ^{11}B which has a proton hole coupled to ^{12}C, the theoretical studies based on antisymmetrized molecular dynamics (AMD) [12,13] pointed out that the $3/2_3^-$ state located just below the ^{7}Li $+ \alpha$ threshold has pronounced $2\alpha + t$ clustering with large radius. Hence, the state was suggested as a candidate of the Hoyle-analog state. More recently, Yamada *et al.* performed the orthogonality condition model (OCM) calculation [14] and predicted the $1/2_2^+$ state as another candidate of the Hoyle-analog state in which all of the 2α and triton particles occupy the s-wave state.

Several discussions have also been made for ^{13}C which has an extra neutron. Yamada *et al.* [15] discussed the possible reduction of spin-orbit splitting in the Hoyle-analog states. Namely, they suggested that the spin-orbit splitting between the $p_{1/2}$ and $p_{3/2}$ coupled to the Hoyle state ($1/2^-$ and $3/2^-$ states) will be reduced, because the splitting is dependent on the first derivative of the density distribution and the Hoyle

state has a dilute density profile. In addition to this, Yamada *et al.* performed the OCM calculation [16] and predicted the Hoyle-analog $1/2^+$ state in which all of three α particles and a neutron occupy the same s-wave state, which is quite similar to the analysis made for ^{11}B. Thus, the $3/2^-$, $1/2^-$, and $1/2^+$ states in ^{13}C are of particular interest and importance for the understanding of the Hoyle-analog state in $N \neq Z$ nuclei.

At present, the existence of the Hoyle-analog $3/2^-$, $1/2^-$, and $1/2^+$ states in ^{13}C is still ambiguous, because the information is not enough to identify them. Therefore, in this work, we conduct the AMD calculation to supply further theoretical information. We investigate the spectroscopic factors (S factors) in ^{12}C $+ n$ and ^{9}Be $+ \alpha$ channels to identify the Hoyle-analog states. Furthermore, we focus on the isoscalar dipole (IS1) transition strength as well as the isoscalar monopole (IS0) transition strength, which are known to be enhanced for the cluster states [12,17–21]. We expect that they are useful to identify the Hoyle-analog states in ^{13}C.

This paper is organized as follows: First, we explain theoretical framework of AMD and how to calculate S factors of the ^{12}C $+ n$ and ^{9}Be $+ \alpha$ channels. Second, we present our numerical calculation results and compare them to experimental data. We analyze nuclear structure of $3/2^-$, $1/2^-$, and $1/2^+$ states in detail using S factors and identify the Hoyle-analog states. We also discuss on the IS0 and IS1 transition strengths to supply theoretical information for forthcoming experiments. Finally, we summarize our paper.

II. AMD FRAMEWORK

A. Hamiltonian and model wave function

The Hamiltonian employed in this work is

$$\hat{H} = \sum_{i=1}^{A} \hat{t}_i - \hat{t}_{\text{c.m.}} + \sum_{i<j} \hat{v}_{NN} + \sum_{i<j} \hat{v}_{\text{Coul}}, \quad (1)$$

where $\hat{t}_i$ is the ith nucleon kinetic energy and $\hat{v}_{NN}$ and $\hat{v}_{\text{Coul}}$ are the Gogny D1S nucleon-nucleon interaction [22] and Coulomb interaction, respectively. The center-of-mass kinetic energy $\hat{t}_{\text{c.m.}}$ is subtracted from the Hamiltonian.

The intrinsic AMD wave function is a Slater determinant of nucleon Gaussian wave packets [23–25],

$$\Phi_{AMD} = \mathcal{A}\{\varphi_1 \varphi_2 \cdots \varphi_A\}, \quad (2)$$

$$\varphi_i = \phi_i \otimes \chi_i \otimes \xi_i, \quad (3)$$

$$\phi_i = \left(\frac{\pi^3}{8|\boldsymbol{\nu}|}\right)^{-\frac{1}{4}} \exp\left[-\sum_{\sigma=xyz} \nu_\sigma \left(r_{i\sigma} - \frac{Z_{i\sigma}}{\sqrt{\nu_\sigma}}\right)\right], \quad (4)$$

$$\chi_i = \alpha_i |\uparrow\rangle + \beta_i |\downarrow\rangle, \quad \xi_i = |p\rangle \text{ or } |n\rangle. \quad (5)$$

It is noted that the center-of-mass wave function $\Phi_{\text{c.m.}}$ is analytically separable from the intrinsic wave function,

$$\Phi_{AMD} = \Phi_{\text{int}} \Phi_{\text{c.m.}}, \quad (6)$$

$$\Phi_{\text{c.m.}} = \left(\frac{\pi^3}{8A^3|\boldsymbol{\nu}|}\right)^{-\frac{1}{4}} \exp\left[-A \sum_{\sigma=xyz} \nu_\sigma R_\sigma^2\right]. \quad (7)$$

Here, Φ_{int} is the internal wave function, and we assume that the relation $\sum_i \boldsymbol{Z}_i = \boldsymbol{0}$ holds. Therefore, the AMD framework is completely free from spurious motion. This is an important advantage when we calculate the IS1 transition strengths. The parameters of the AMD wave function $\boldsymbol{\nu}$, $\boldsymbol{Z}_i$, α_i, and β_i are determined so as to minimize the energy after parity-projection,

$$\Phi^\pi = \frac{1 + \pi \hat{P}_x}{2} \Phi_{\text{int}}, \quad \pi = \pm, \quad (8)$$

$$E^\pi = \frac{\langle \Phi^\pi | \hat{H} | \Phi^\pi \rangle}{\langle \Phi^\pi | \Phi^\pi \rangle}. \quad (9)$$

To describe the various states of ^{13}C, we impose the constraint on the expectation values of harmonic oscillator quanta N, λ, and μ, which are defined by using the harmonic oscillator quanta in Cartesian coordinates N_x, N_y, and N_z:

$$N = N_x + N_y + N_z, \quad \lambda = N_z - N_y, \quad \mu = N_y - N_x. \quad (10)$$

Here, we assume the relation $N_x \leqslant N_y \leqslant N_z$. Roughly speaking, the excitation of system is expressed by N, and λ and μ indicate the asymmetries around the longest and shortest deformed axis. The details of this constraint are described in Ref. [26].

Compared with the constraint on the quadrupole deformation parameters ($\beta\gamma$ constraint), which is often used in mean-field and AMD calculations, the constraint on N, λ, and μ is appropriate for the description of the highly excited states. The $\beta\gamma$ constraint is useful to describe the low-lying quadrupole collectivity but it often fails to describe highly excited states. On the other hand, the constraint on N, λ

and μ is capable of describing the highly excited states with many-particle many-hole configurations. In this study, the possible combinations of values for N, λ, and μ up to $N = 18$ ($9\hbar\omega$ excitation) are adopted as the constraint. We denote thus-obtained basis wave function as $\Phi^\pi(N\lambda\mu)$.

After energy variation, the basis wave functions are projected to angular-momentum eigenstates and superposed to obtain excitation spectra and eigen wave functions [generator coordinate method (GCM)]:

$$\Phi_{MK}^{J\pi}(N_i\lambda_i\mu_i) = \mathcal{N}_K^{-\frac{1}{2}} \hat{P}_{MK}^J \Phi^\pi(N_i\lambda_i\mu_i), \quad (11)$$

$$\mathcal{N}_K = \langle \Phi_{MK}^{J\pi}(N\lambda\mu) | \Phi_{MK}^{J\pi}(N\lambda\mu) \rangle, \quad (12)$$

$$\Psi_n^{J\pi} = \sum_{Ki} g_{Kin}^{J\pi} \Phi_{MK}^{J\pi}(N_i\lambda_i\mu_i), \quad (13)$$

where $\hat{P}_{MK}^J$ is the angular momentum projection operator. The coefficients $g_{Kin}^{J\pi}$ is determined by diagonalizing the Hamiltonian,

$$\sum_{i'K'} H_{iKi'K'}^{J\pi} g_{i'K'n}^{J\pi} = E_n^{J\pi} \sum_{i'K'} N_{iKi'K'}^{J\pi} g_{i'K'n}^{J\pi}, \quad (14)$$

$$H_{iKi'K'}^{J\pi} = \langle \Phi_{MK}^{J\pi}(N_i\lambda_i\mu_i) | \hat{H} | \Phi_{MK'}^{J\pi}(N_{i'}\lambda_{i'}\mu_{i'}) \rangle, \quad (15)$$

$$N_{iKi'K'}^{J\pi} = \langle \Phi_{MK}^{J\pi}(N_i\lambda_i\mu_i) | \Phi_{MK'}^{J\pi}(N_{i'}\lambda_{i'}\mu_{i'}) \rangle. \quad (16)$$

B. Reduced width amplitudes and spectroscopic factors

To search for Hoyle-analog states, we calculate the reduced width amplitudes and S factors in the ^{12}C + n and ^{9}Be + α channels. The reduced width amplitude in the ^{12}C + n channel is defined as

$$y_{j_C\pi_C jl}^{J\pi n}(a) = \sqrt{13} \left\langle \frac{\delta(r-a)}{r^2} \left[\Phi_C^{j_C\pi_C} [Y_l(\hat{r})\chi_{1/2}]_j \right]_J \middle| \Psi_n^{J\pi} \right\rangle, \quad (17)$$

where $\Phi_C^{j_C\pi_C}$ is the wave function of ^{12}C and $\chi_{1/2}$ is the spin-isospin wave function of the neutron. j_C and π_C are angular momentum and parity of ^{12}C, and j and l are total and orbital angular momenta of the neutron. In a same manner, the reduced width amplitude in the ^{9}Be + α channel is defined as

$$y_{j_{Be}\pi_{Be}l}^{J\pi n}(a) = \sqrt{\frac{13!}{9!4!}} \left\langle \frac{\delta(r-a)}{r^2} \Phi_\alpha \left[\Phi_{Be}^{j_{Be}\pi_{Be}} Y_l(\hat{r}) \right]_J \middle| \Psi_n^{J\pi} \right\rangle, \quad (18)$$

where $\Phi_{Be}^{j_{Be}\pi_{Be}}$ is the wave function of ^{9}Be with angular momentum j_{Be} and parity π_{Be}. Φ_α is the wave function of the ground state of the α cluster. The S factors of the ^{12}C + n and ^{9}Be + α channels are defined as the integrals of the reduced width amplitudes,

$$S_{j_C\pi_C jl}^{J\pi n} = \int_0^\infty da \left| a y_{j_C\pi_C jl}^{J\pi n}(a) \right|^2, \quad (19)$$

$$S_{j_{Be}\pi_{Be}l}^{J\pi n} = \int_0^\infty da \left| a y_{j_{Be}\pi_{Be}l}^{J\pi n}(a) \right|^2. \quad (20)$$

To evaluate the reduced width amplitudes, we use the Laplace expansion method proposed in Ref. [27], which can treat the deformed and the excited cluster wave functions
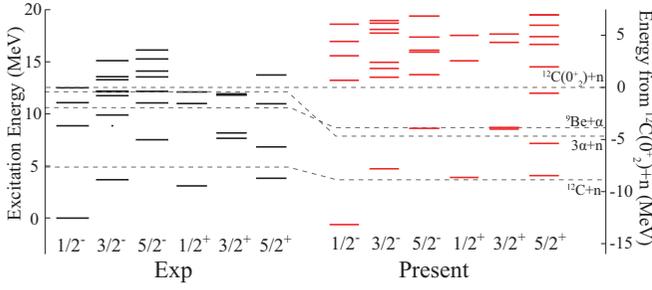
FIG. 1. The calculated and observed [28] excitation spectra of the $1/2^\pm$, $3/2^\pm$, and $5/2^\pm$ states of ¹³C with the threshold energies for the relevant channels. The calculated threshold energies from the ¹²C(0_2^+) + n threshold are -5.4 MeV for ¹²C(2_1^+) + n, 4.2 MeV for ¹²C(2_2^+) + n, -1.9 MeV for ⁹Be($5/2_1^-$) + n, -1.7 MeV for ⁹Be($1/2_1^-$) + n, and -2.0 MeV for ⁹Be($1/2_1^+$) + n channels.

without any approximations. In this study, the α cluster is described by the $(0s)^4$ configuration with oscillator parameter $\nu = m\omega/(2\hbar) = 0.25$ fm^{-1} while the wave functions of ⁹Be and ¹²C are obtained by AMD + GCM calculations.

III. RESULTS AND DISCUSSIONS

A. Excitation spectra

We performed the energy variation under constraint on the harmonic oscillator quanta N, λ and μ. Using the basis wave functions generated by the energy variation, we performed the GCM calculation and obtained excitation spectra of ¹³C. The observed data [28] and calculated excitation spectra up to $E_x = 20$ MeV with $J^\pi \leqslant 5/2^\pm$ are shown in Fig. 1.

The calculated yrast states reasonably agree with the observed spectra. On the other hand, the energies of the non-yrast states above 10 MeV are overestimated. For example, the $3/2_2^-$ state observed at 9.9 MeV is located at 13.2 MeV in the present calculation. As shown later, many of the excited states located above 10 MeV have cluster structure. Thus, we can say that the present calculation overestimates the energies of the cluster states. This is mainly due to the limitation of our model space. The restriction up to $N = 18$ configuration may not be sufficient to describe the relative motion of clusters.

B. Structure of $1/2^-$ states

In this section, we discuss the structure of the $1/2^-$ states, which are the candidates of the Hoyle-analog state having ¹²C(0_2^+) ⊗ $p_{1/2}$ configuration. The calculated root-mean-square (rms) radii, S factors in the ¹²C + n and ⁹Be + α channels, and the IS0 transition matrix from the ground state M(IS0) are shown in Fig. 2. The transition matrix is defined as

$$\mathcal{M}^{\mathrm{IS0}} = \sum_{i=1}^{A} (\boldsymbol{r}_i - \boldsymbol{r}_{\mathrm{c.m.}})^2, \quad \boldsymbol{r}_{\mathrm{c.m.}} = \frac{1}{A} \sum_i \boldsymbol{r}_i, \quad (21)$$

$$M(\mathrm{IS0}) = \left| \langle \Psi_k^{1/2^-} | \mathcal{M}^{\mathrm{IS0}} | \Psi_1^{1/2^-} \rangle \right|. \quad (22)$$

The ground state ($1/2_1^-$ state) has the compact shell structure with a radius of 2.52 fm. This state has large overlap (0.94) with the basis wave function obtained by energy vari-
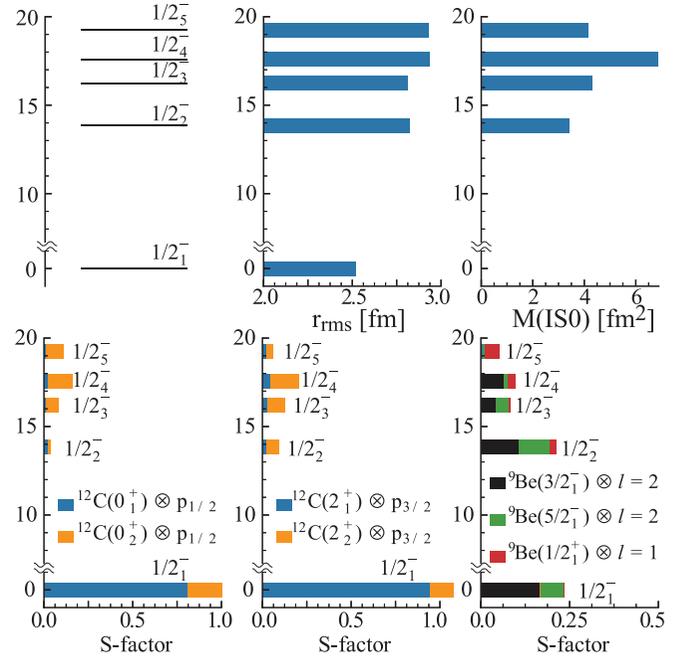
FIG. 2. The excitation energies and the properties of the $1/2^-$ states obtained in the present work. In the upper panels, the calculated excitation spectra, matter rms radii r_{rms}, and IS0 transition matrix from the ground state M(IS0) are shown from left to right. The calculated S factors in the ¹²C + n and ⁹Be + α channels are presented in the lower panels. In the last panel, l denotes the orbital angular momentum between α and ⁹B clusters.

ation with the constraint $(N, \lambda, \mu) = (9, 0, 3)$; its intrinsic density distribution is shown in Fig. 3(a). The shell-model like character of the ground state can be confirmed by the large S factors in the ¹²C(0_1^+) ⊗ $p_{1/2}$ and ¹²C(2_1^+) ⊗ $p_{3/2}$ channels, which are 0.81 and 0.94 respectively. It is noted that ¹²C(0_1^+) ⊗ $p_{1/2}$ and ¹²C(2_1^+) ⊗ $p_{3/2}$ channels identically correspond to $(0s)^4(0p_{3/2})^8(0p_{1/2})^1$ configuration if the ¹²C(0_1^+) and ¹²C(2_1^+) have the $(0s)^4(0p_{3/2})^8$ and $(0s)^4(0p_{3/2})^7(0p_{1/2})^1$ configurations, respectively.

While the ground state has the compact shell structure, the excited $1/2^-$ states have rms radii larger than 2.70 fm. The enhancement of the rms radii in the excited $1/2^-$ states implies their developed cluster structure. The $1/2_2^-$ state at $E_x = 13.8$ MeV largely overlaps with a wave function having ⁹Be + α cluster configuration, shown in Fig. 3(b), which amounts to 0.46. Hence, this state has large S factors in the ⁹Be($3/2_1^-$) ⊗ $l = 2$ and ⁹Be($5/2_1^-$) ⊗ $l = 2$ channels, which are 0.11 and 0.09, respectively. The RWAs in the ⁹Be($3/2^-$) ⊗ $l = 2$ and ⁹Be($5/2^-$) ⊗ $l = 2$ channels have two nodes ($N = 6$), as shown in Fig. 4(b), while the those in the ground state have one node ($N = 4$). This means that the $1/2_2^-$ state is regarded as the nodal excitation of the intercluster motion between ⁹Be and α clusters. Therefore, the $1/2_2^-$ state is not a Hoyle-analog state but an excited ⁹Be + α cluster state, although it also has non-negligible S factors in the ¹²C + n channels.

The $1/2_3^-$, $1/2_4^-$, and $1/2_5^-$ states have large overlap with the basis wave functions displayed in
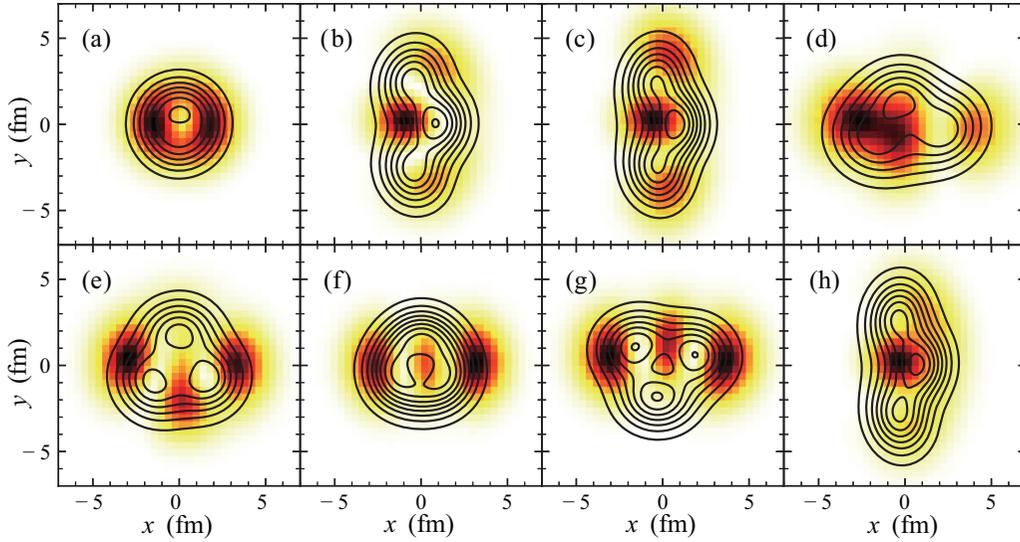
FIG. 3. Intrinsic matter and valence neutron density distributions on the $z = 0$ plane for the basis wave functions obtained with variation under the constraint on the H.O. quanta. The contour plot indicates the matter density distribution while the color plot indicates the valence neutron density distribution. The panels (a)–(e) are the dominant components of the $1/2_1^-$, $1/2_2^-$, $1/2_3^-$, $1/2_4^-$, and $1/2_5^-$ states, respectively. The panels (f)–(h) are those of the $1/2_1^+$, $1/2_2^+$, and $1/2_3^+$ states, respectively.

Figs. 3(c), 3(d), and 3(e), respectively. These states have non-negligible S factors in the $^{12}\text{C}(0_2^+) \otimes p_{1/2}$ channel but the magnitudes are less than 0.20. This means that the $^{12}\text{C}(0_2^+) \otimes p_{1/2}$ configuration (Hoyle-analog configuration) does not manifest as a single excited state, but it is fragmented into these $1/2^-$ states. Thus, we conclude that there is no Hoyle-analog $1/2^-$ state. Interestingly, these states also have the S factors in the $^{12}\text{C}(2_2^+) \otimes p_{1/2}$ channel, which corresponds to the rotational excited state of the Hoyle state. The differences between the $1/2_3^-$, $1/2_4^-$, and $1/2_5^-$ states are seen in different magnitudes of the coupling to the $^9\text{Be} + \alpha$ channels. Similar result was also obtained by Yamada *et al.* [16]. They argued that Hoyle-analog state does not appear in the $1/2^-$ states because of the enhanced $^9\text{Be} + \alpha$ correlation induced by the attractive odd-parity α-n interaction. We also confirm this on account of the non-negligible S-factors in the $^{12}\text{C}(0_2^+) \otimes p_{1/2}$, $^{12}\text{C}(2_2^+) \otimes p_{3/2}$ and $^9\text{Be} + \alpha$ channels. In addition, our result shows the shrinkage of the rms radii compared to the Hoyle state (2.94 fm), which is also consistent with the interpretation suggested by Yamada *et al.* [16].

Although there is no Hoyle-analog state, it is interesting to note that all of the four $1/2^-$ states have a large monopole transition matrix comparable with the Hoyle state, which, in total, exhaust 24% of the energy weighted sum rule, which is consistent with the experimental results [29–31]. One may wonder why the number of excited states with a large monopole matrix is increased in ^{13}C rather than in ^{12}C despite the fragmentation of the $^{12}\text{C}(0_2^+) \otimes 0p_{1/2}$ configuration into many states. The reason for the increase and the origin of the monopole strength of each state are explained as follows.

The origin of the monopole strength of the $1/2_2^-$ state is the excitation of the relative motion between ^9Be and α clusters. As already mentioned, the $1/2_2^-$ state has a $^9\text{Be} + \alpha$ cluster structure in which the intercluster motion

is excited by $2\hbar\omega$ from the ground state. Therefore, it naturally has the enhanced monopole strength. Differently from the $1/2_2^-$ state, the monopole strengths of the other $1/2^-$ states originate in the excitation of the ^{12}C core. In particular, we found that the monopole excitation of $^{12}\text{C}(2_1^+) \rightarrow {}^{12}\text{C}(2_2^+)$ plays an important role, as does the excitation of $^{12}\text{C}(0_1^+) \rightarrow {}^{12}\text{C}(0_2^+)$. To elucidate this, we here show a simple estimation of the monopole transition matrix. First, let us assume that the ground state of ^{13}C (the $1/2_1^-$ state) has a $(0s_{1/2})^4(0p_{3/2})^8(0p_{1/2})^1$ configuration, and $^{12}\text{C}(0_1^+)$ and $^{12}\text{C}(2_1^+)$ respectively have $(0s_{1/2})^4(0p_{3/2})^8$ and $(0s_{1/2})^4(0p_{3/2})^7(0p_{1/2})^1$ configurations. Then, $^{13}\text{C}(1/2_1^-)$ can be written as

$$|{}^{13}\text{C}(1/2_1^-)\rangle = n_0 |\mathcal{A}\{{}^{12}\text{C}(0_1^+) \otimes 0p_{1/2}\}\rangle, \qquad (23)$$

$$= n_2 |\mathcal{A}\{{}^{12}\text{C}(2_1^+) \otimes 0p_{3/2}\}\rangle, \qquad (24)$$

where n_0 and n_2 denote the normalization factors defined as

$$n_0 = \langle \mathcal{A}\{{}^{12}\text{C}(0_1^+) \otimes 0p_{1/2}\} | \mathcal{A}\{{}^{12}\text{C}(0_1^+) \otimes 0p_{1/2}\}\rangle^{-1/2}, \quad (25)$$

$$n_2 = \langle \mathcal{A}\{{}^{12}\text{C}(2_1^+) \otimes 0p_{3/2}\} | \mathcal{A}\{{}^{12}\text{C}(2_1^+) \otimes 0p_{3/2}\}\rangle^{-1/2}. \quad (26)$$

Second, the other excited $1/2^-$ states ($1/2_3^-$, $1/2_4^-$ and $1/2_5^-$) may be written as

$$
\begin{aligned}
|{}^{13}\text{C}(1/2_{\text{ex}}^-)\rangle = {} & an_0' |\mathcal{A}\{{}^{12}\text{C}(0_2^+) \otimes 0p_{1/2}\}\rangle \\
& + bn_2' |\mathcal{A}\{{}^{12}\text{C}(2_2^+) \otimes 0p_{3/2}\}\rangle \\
& + (\text{other configurations})
\end{aligned}
\qquad (27)
$$

since they are dominated by the $^{12}\text{C}(0_2^+) \otimes 0p_{1/2}$ and $^{12}\text{C}(2_2^+) \otimes 0p_{3/2}$ configurations. Here, n_0' and n_2' are the normalization factors defined in a similar manner, and we assumed that the neutron orbits are unchanged from the ground state. We also assume that $n_0'|\mathcal{A}\{{}^{12}\text{C}(0_1^+) \otimes 0p_{1/2}\}$
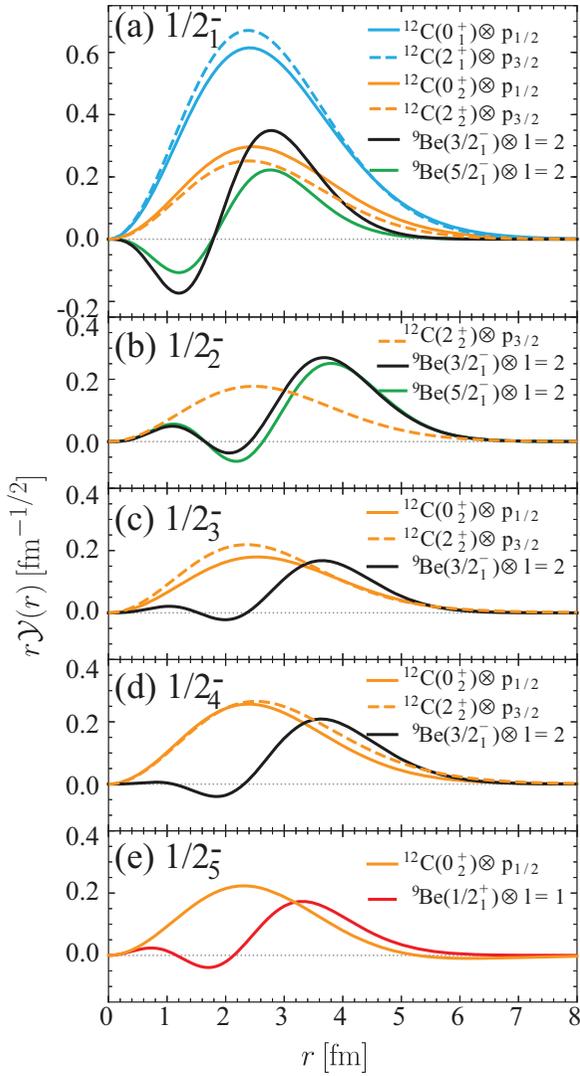
FIG. 4. The calculated RWAs of the $1/2^-$ states in the ^{12}C $+ n$ and ^{9}Be $+ \alpha$ channels. The RWAs that yield S larger than 0.04 are displayed.

FIG. 5. The calculated excitation spectra, the rms matter radii $r_{\rm rms}$, and the S factors of $3/2^-$ states below 20 MeV. The S factors smaller than 0.05 are not displayed.

and $n_2'|\mathcal{A}\{^{12}\text{C}(2_1^+) \otimes 0p_{3/2}\}\rangle$ are orthogonal, and their amplitudes are represented by a and b.

Finally, following the discussion by Yamada *et al.* [18], we rewrite the monopole operator as

$$\mathcal{M}^{\rm IS0}(^{13}\text{C}) = \mathcal{M}^{\rm IS0}(^{12}\text{C}) + \frac{12}{13}r^2, \tag{28}$$

where $\mathcal{M}^{\rm IS0}(^{12}\text{C})$ acts on the ^{12}C core, while $\boldsymbol{r}$ denotes the coordinate between the ^{12}C core and valence neutron. With these expressions, we can derive an estimation for the monopole transition matrix,

$$M(\text{IS0}) = \langle^{13}\text{C}(1/2^-_{\rm ex})|\mathcal{M}^{\rm IS0}(^{13}\text{C})|^{13}\text{C}(1/2_1^-)\rangle$$

$$= a^* \frac{n_0'}{n_0} \langle^{12}\text{C}(0_2^+)|\mathcal{M}^{\rm IS0}(^{12}\text{C})|^{12}\text{C}(0_1^+)\rangle$$

$$+ b^* \frac{n_2'}{n_2} \langle^{12}\text{C}(2_2^+)|\mathcal{M}^{\rm IS0}(^{12}\text{C})|^{12}\text{C}(2_1^+)\rangle$$

$$+ \text{(other channels)}. \tag{29}$$

The derivation of the Eq. (29) is almost same as that explained in Ref. [18]. Thus, the monopole strengths of the excited $1/2^-$ states can be related to the monopole transitions of ^{12}C. Here, it is noted that n_0'/n_0 and n_2'/n_2 are almost equal to 1, and $\langle^{12}\text{C}(2_2^+)|\mathcal{M}^{\rm IS0}(^{12}\text{C})|^{12}\text{C}(2_1^+)\rangle$ is as large as or even larger than $\langle^{12}\text{C}(0_2^+)|\mathcal{M}^{\rm IS0}(^{12}\text{C})|^{12}\text{C}(0_1^+)\rangle$. Therefore, if a and b are not small and have the same phase, the transition matrix can be large. From this simple estimation, it is also clear that the ^{12}C$(2_2^+) \otimes 0p_{3/2}$ channel increases the number of $1/2^-$ states having large monopole transition strengths.

C. Structure of the $3/2^-$ states

The $3/2^-$ states are also candidates of the Hoyle-analog state with a P-wave valence neutron. The properties of the $3/2^-$ states below 20 MeV are summarized in Fig. 5. In our calculation, except for the $3/2_1^-$ and $3/2_4^-$ states, the $3/2^-$ states have matter rms radius larger than 2.75 fm.

The $3/2_1^-$ state is obviously dominated by the ^{12}C$(2_1^+) \otimes p_{1/2}$ channel ($S = 0.87$), and its configuration is concluded to be $(0p_{3/2})^{-1}(0p_{1/2})^2$ because ^{12}C(2_1^+) is dominated by the $(0p_{3/2})^{-1}(0p_{1/2})^1$ configuration. The properties of the other $3/2^-$ states are not clear, since their S factors are small in all calculated channels ($S \leqslant 0.14$). In particular, there are no states having sizable S factor in the ^{12}C$(0_2^+) \otimes p_{3/2}$ channel except for the $3/2_1^-$ state. Therefore, we conclude that there is no Hoyle-analog $3/2^-$ state below 20 MeV.

As explained above, the Hoyle-analog state with a P-wave neutron does not appear. This is due to the strong attractive interaction between the α cluster and the P-wave neutron, which induces the coupling with many different channels. As
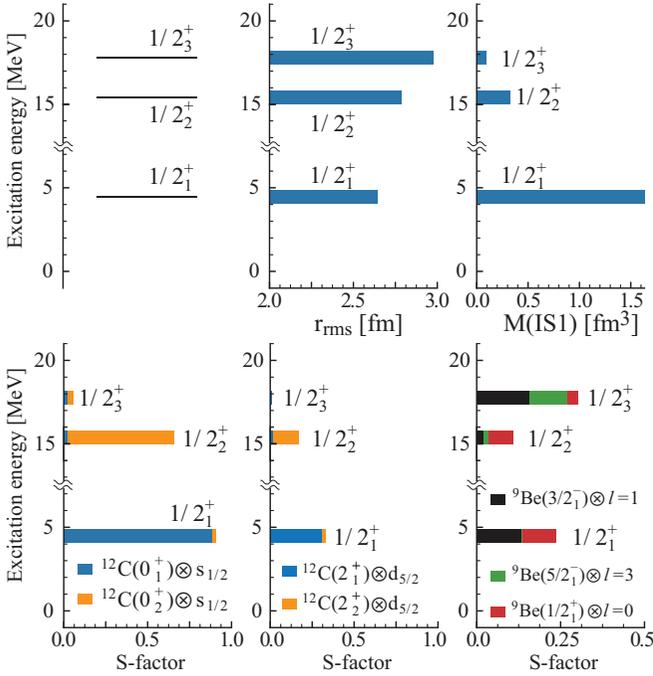
FIG. 6. The calculated excitation spectra, matter rms radii, $M(\text{IS1})$, and S factors of $1/2^+$ states below 20 MeV are shown in the same manner as in Fig. 2.

a result, the $^{12}\text{C}(0_2^+) \otimes p_{1/2}$ and $^{12}\text{C}(0_2^+) \otimes p_{3/2}$ configurations are fragmented into many states.

D. Structure of the $1/2^+$ states

In the above discussion, we showed that there is no Hoyle-analog state in the $1/2^-$ and $3/2^-$ states, where the strong attractive interaction between α clusters and the neutron induces coupling with many different channels. On other hand, because the interaction between the α and the S-wave neutron is weaker than that for the P-wave neutron, we expect that the $1/2^+$ state is a promising candidate of the Hoyle-analog state.

The calculated rms radii and S factors are shown in Fig. 6. The rms radius of the $1/2_1^+$ state is only 2.62 fm and suggests that the $1/2_1^+$ state has a compact shell structure. In fact, the $1/2_1^+$ state has the largest overlap with the basis wave function, having the shell structure shown in Fig. 3(f). On the other hand, the radii of the $1/2_2^+$ and $1/2_3^+$ states are larger than 2.75 fm, which indicates their developed cluster structure. This point can be clearly confirmed by analysis of the S factor. The $1/2_1^+$ state is a particle-hole excited state, because its S factor in the $^{12}\text{C}(0_1^+) \otimes s_{1/2}$ channel is 0.84 and the other channel contributions are relatively small. The RWA of the $1/2_1^+$ state in the $^{12}\text{C}(0_1^+) \otimes s_{1/2}$ has one node [Fig. 7(a)], and hence its particle-hole configuration is $(0p_{1/2})^{-1}(1s_{1/2})^1$.

The $1/2_2^+$ state is located 3.0 MeV above $^{12}\text{C}(0_2^+) + n$ threshold energy and has the largest S factor, 0.64, in the $^{12}\text{C}(0_2^+) \otimes s_{1/2}$ channel among the calculated $1/2^+$ states. The RWA in the $^{12}\text{C}(0_2^+) \otimes s_{1/2}$ channel has one node
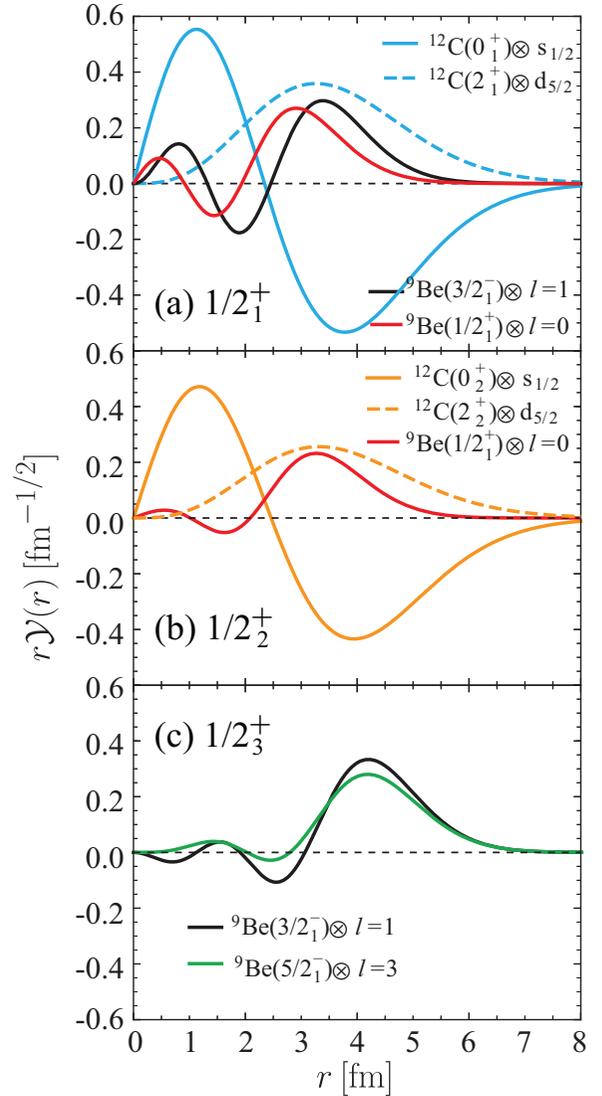
FIG. 7. The calculated RWAs of the $1/2^+$ states in the $^{12}\text{C} + n$ and $^9\text{Be} + \alpha$ channels. The RWAs which yields the larger S than 0.04 are displayed.

[Fig. 7(b)], which indicates that the $1/2_2^+$ state is the Hoyle-analog $1/2^+$ state with $^{12}\text{C}(0_2^+) \otimes 1s_{1/2}$ configuration. It has the largest overlap with the basis wave function shown in Fig. 3(g), but its magnitude is 0.48. This state also has non-negligible overlaps with the various basis wave functions having $3\alpha + n$ cluster structure, which suggests the dilute gaslike nature of the $1/2_2^+$ state. However, the rms radius of the $1/2_2^+$ state (2.76 fm) is reduced compared to that of the Hoyle state (2.94 fm) in our calculation. This shrinkage indicates that the Hoyle-analog nature is weakened by the interaction between ^{12}C and the valence neutron. This point can be seen in the coupling with the other $^{12}\text{C} + n$ channels. For example, the $1/2_2^+$ state has the non-negligible S factors of 0.11 and 0.18 in the $^{12}\text{C}(1_1^-) \otimes p_{3/2}$ and $^{12}\text{C}(2_2^+) \otimes d_{5/2}$ channels, respectively. It is also noted that the present result is inconsistent with the OCM calculation [16], which concluded
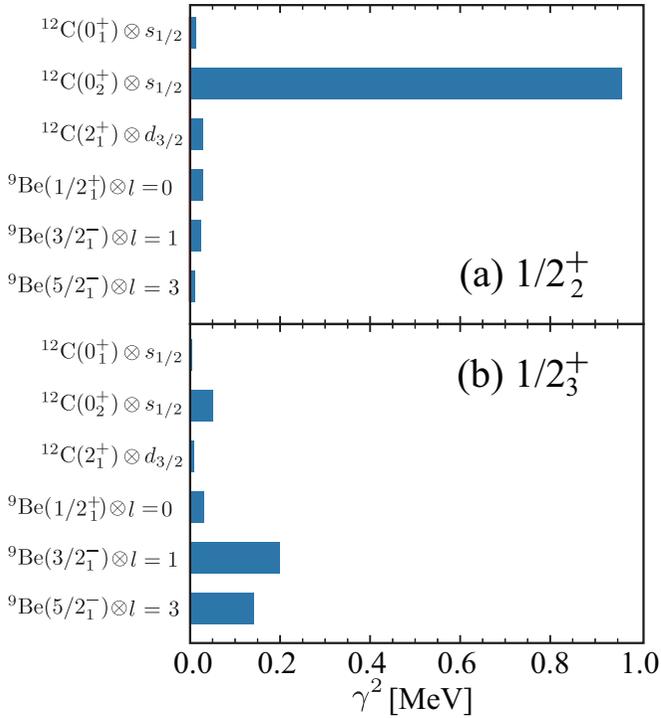
FIG. 8. The calculated reduced widths γ^2 of the $1/2_2^+$ and $1/2_3^+$ states for ^{12}C $+ n$ and ^{9}Be $+ \alpha$ channels. The matching radius $a = 4.5$ fm is applied.

the $1/2_5^+$ state is a Hoyle-analog state. We will revisit this problem in Sec. III E.

The $1/2_3^+$ state has quite different nature from the $1/2_1^+$ and $1/2_2^+$ states. This state has almost zero S factors in the ^{12}C $+ n$ channels shown in Fig. 6, but the S factors in the ^{9}Be $+ \alpha$ channels amount to 0.32 in total. Therefore, we conclude that the $1/2_3^+$ state has the ^{9}Be $+ \alpha$ cluster structure. Interestingly, its density distribution [Fig. 3(h)] shows a structure similar to to the $1/2_2^-$ state [Fig. 3(b)]. Furthermore, the S factors indicate that they are dominated by the ^{9}Be($3/2_1^-$) $+ \alpha$ and ^{9}Be($5/2_1^-$) $+ \alpha$ channels. Therefore, we consider that the $1/2_2^-$ and $1/2_3^+$ state constitute a parity doublet having the

^{9}Be $+ \alpha$ cluster structure. A similar bent-armed $3\alpha + n$ cluster structure in negative parity states was also discussed by Furutachi *et al.* [32] in relation to the inversion doublet of the ^{9}Be $+ \alpha$ cluster band suggested by Millin and von Oertzen [33]. In addition to this, it is worthwhile to mention that the $1/2_3^+$ state also has non small S factor in the ^{12}C(1_1^-) $\otimes p_{3/2}$ channel. Note that a previous AMD calculation [34] predicted the bent-armed linear-chain-like structure of the 1_1^- and 0_3^+ states of ^{12}C, and hence the $1/2_3^+$ state naturally has the S factor in the ^{12}C(1_1^-) channel. However, the $1/2_3^+$ state does not have an S factor in the ^{12}C(0_3^+) $\otimes s_{1/2}$ channel. This may be due to the lack of the low energy s orbit for the valence neutron around the bent-armed linear chain, as the lowest ones are already occupied by the nucleons in the α clusters.

The calculated IS1 transition matrix M(IS1) (Fig. 6) indicates that the $1/2_1^+$ state is strongly populated by IS1 transition from the ground state [M(IS1) = 0.95 W.u.] while the $1/2_2^+$ and $1/2_3^+$ states are not. In particular, despite of its Hoyle-analog structure, the IS1 transition strength of the $1/2_2^+$ state is unexpectedly small. This may be explained as follows. Following the discussion in Refs. [20,35], we decompose the system into the ^{12}C core and the valence neutron, and rewrite the IS1 operator as

$$
\mathcal{M}_\mu^{IS1} = \frac{132}{169} r^2 \mathcal{Y}_{1\mu}(\boldsymbol{r}) - \frac{5}{39} \sum_{i \in {}^{12}\mathrm{C}} \xi_i^2 \mathcal{Y}_{1\mu}(\boldsymbol{r})
$$

$$
+ \frac{4\sqrt{2\pi}}{39} \left[\sum_{i \in {}^{12}\mathrm{C}} \mathcal{Y}_2(\boldsymbol{\xi}_i) \otimes \mathcal{Y}_1(\boldsymbol{r}) \right]_{1\mu} + \sum_{i \in {}^{12}\mathrm{C}} \xi_i^2 \mathcal{Y}_{1\mu}(\boldsymbol{\xi}_i),
$$

(30)

where $\boldsymbol{\xi}_i$ denote the internal coordinates of the ^{12}C core, while $\boldsymbol{r}$ denotes the valence neutron coordinate. The first term of Eq. (30) is dependent only on $\boldsymbol{r}$ and induces the IS1 transition of the valence neutron. Therefore, the $1/2_1^+$ state, which has the one-particle–one-hole (1p1h) configuration, is mainly excited by this term. This is the reason why $1/2_1^+$ state has a strong IS1 transition matrix comparable with the Weisskopf estimate.
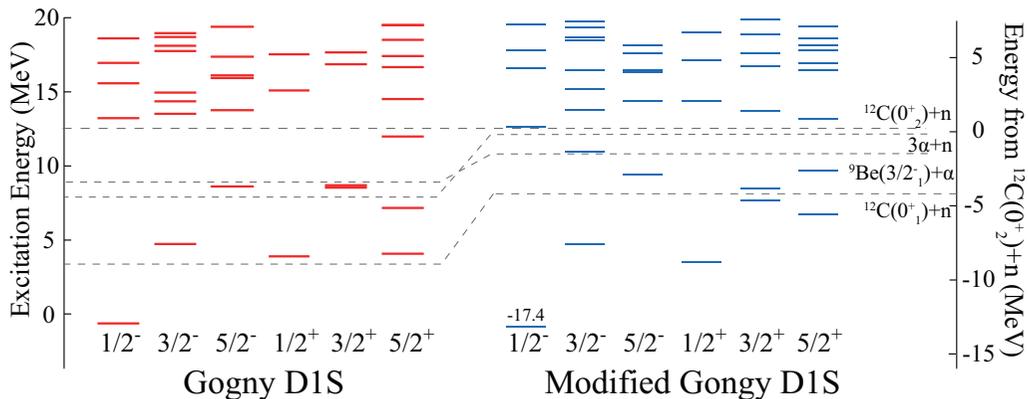
FIG. 9. The comparison between the excitation spectra of the $1/2^\pm$, $3/2^\pm$, and $5/2^\pm$ states of ^{13}C calculated with Gogny D1S (red) and modified Gogny D1S (blue) interactions.
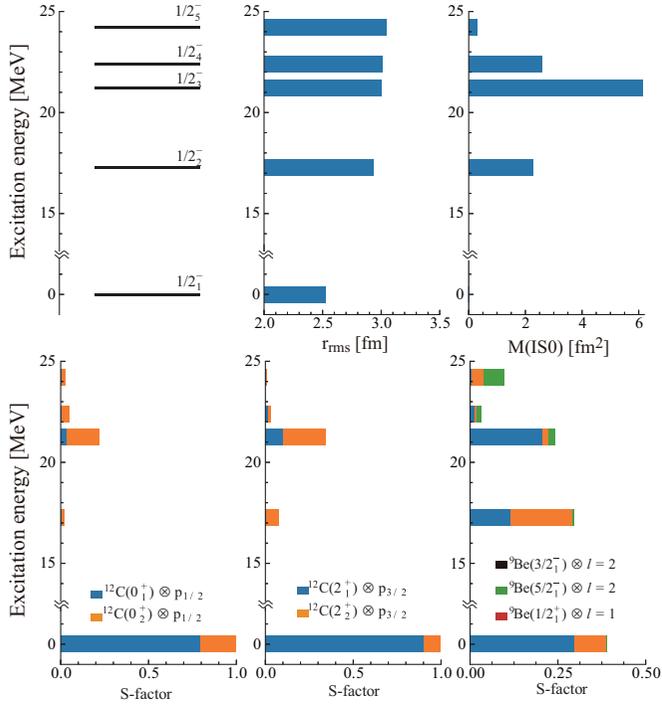
FIG. 10. Same with Fig. 4 but obtained by using the modified Gogny D1S interaction.

FIG. 11. Same as Fig. 7 but obtained by using the modified Gogny D1S interaction.

On the other hand, the second and third terms induce the monopole and quadrupole transitions of ^{12}C core. Therefore, if these terms act on the ground state wave function [Eq. (30)], they bring about the core excitations $^{12}C(0_1^+) \to {}^{12}C(0_2^+)$ and $^{12}C(2_1^+) \to {}^{12}C(0_2^+)$ combined with the valence neutron excitations to yield the Hoyle-analog $1/2_2^+$ state. Since the transition matrix for the core excitations are large, we expect that the IS1 excitation from the ground state to the $1/2_2^+$ state is enhanced. However, the coefficients for these two terms are rather small ($5/39$ and $4\sqrt{2\pi}/39$). As a result, the $1/2_2^+$ state has relatively small transition strength despite its dilute gaslike nature.

Thus, the Hoyle-analog $1/2_2^+$ state has unexpectedly small $M(IS1)$. However, in the preliminary reported IS1 transition strength distribution of ^{13}C, there is a small peak around 13 MeV [29–31], which is close to our prediction and may correspond to the Hoyle-analog $1/2_2^+$ state.

Finally, we discuss the decay width of the $1/2^+$ states. Owing to the cluster structure of the $1/2_2^+$ and $1/2_3^+$ states, they have unique decay patterns. The calculated reduced widths γ^2 of the $1/2_2^+$ and $1/2_3^+$ states in the ^{12}C $+ n$ and ^{9}Be $+ \alpha$ channels are shown in Fig. 8. The $1/2_2^+$ state has largest reduced width of 0.96 MeV in the $^{12}C(0_2^+) \otimes s_{1/2}$ channel. The reduced widths in the other channels are negligibly small. On the other hand, The reduced decay widths in the ^{9}Be$(3/2_1^-) \otimes l = 1$ and ^{9}Be$(5/2_1^-) \otimes l = 3$ channels are largest in the $1/2_3^+$ state. Because of the larger Q value, the $1/2_3^+$ state dominantly decays via the ^{9}Be$(3/2_1^-) \otimes l = 1$ channel. Therefore, the strong decays via the $^{12}C(0_2^+) \otimes s_{1/2}$ and ^{9}Be$(3/2_1^-) \otimes l = 1$ channels are signatures of the $1/2_2^+$ and $1/2_3^+$ states, respectively.

E. Interaction dependence of the results

The major problem of the results discussed above is that the threshold energies of various cluster channels are not reproduced correctly. This mainly due to the limitation of the present model space and the Gogny D1S effective interaction used in this study. In particular, the Gogny D1S interaction does not reproduce the energy of the Hoyle state. As a result (see Fig. 1) the energies of the highly excited cluster states are overestimated and there is an energy gap between the highly excited cluster states and the low-lying shell-like states ($1/2_1^\pm$, $3/2_1^\pm$, $5/2^\pm$, $3/2_2^+$, and $5/2_2^+$ states). Therefore, one may doubt that the discussion about the structure of the Hoyle-analog state will be qualitatively changed if we employ a different effective interaction.

Therefore, in this section, we discuss the interaction dependence of the Hoyle-analog state. For this purpose, we modified the Wigner and Majorana parameters of the central part of the Gogny D1S interaction by multiplying with factors of 1.02 and 0.98, respectively. This modification reproduces the energy of the Hoyle state measured from the 3α threshold energy. The spectra calculated by this modified interaction are shown in Fig. 9. One can see that the energy gap between the low-lying shell-like states and the highly excited cluster states are reduced and are close to the observations, although the

ground state is overbound by 5 MeV. The calculated S factors, rms matter radii, and IS strengths of the $1/2^{\pm}$ states are shown in Figs. 10 and 11. Unexpectedly, we found that the properties of the excited cluster states are not qualitatively changed by the change of the effective interaction. In particular, the $1/2_2^+$ state is still dominated by the ^{12}C$(0_2^+) \otimes s_{1/2}$ channel and is regarded as a Hoyle-analog state, contradicting the OCM calculation [16]. Thus, the properties of the excited cluster states are unchanged by the modification of the interaction, and we consider that the inconsistency between the OCM and AMD results about the $1/2^+$ states originates in the difference of the model space or the difference between the macroscopic and microscopic nuclear models, which should be resolved in future works.

IV. SUMMARY

We studied the Hoyle-analog states in ^{13}C based on AMD. The basis wave functions are obtained by the energy variation with constraint on the expectation values of harmonic oscillator quanta. Using these basis wave functions, the GCM calculation was performed to obtain the excitation energies and the eigen wave functions.

The analysis of the S factors in the ^{12}C $+ n$ and ^{9}Be $+ \alpha$ channels revealed the characters of the ground and excited states of ^{13}C. The ground state ($1/2_1^-$ state) has the $(0s)^4(0p_{3/2})^8(0p_{1/2})^1$ configuration, and the $3/2_1^-$ and $1/2_1^+$ states have the 1p1h configurations. In contrast to these shell-model-like states, the non-yrast states have developed cluster structures. The $1/2_2^-$ and $1/2_3^+$ states constitute the inversion doublet of the bent-armed ^{9}Be $+ \alpha$ cluster structure. The $1/2_3^-$, $1/2_4^-$, and $1/2_5^-$ states are $3\alpha + n$ cluster states in which the ^{12}C$(0_2^+) \otimes 0p_{1/2}$ and ^{12}C$(2_2^+) \otimes 0p_{3/2}$ configurations are mixed. However, they cannot be regarded as the Hoyle-analog state because the S factors in the ^{12}C$(0_2^+) \otimes p_{1/2}$ channel are small. Similarly, there is no Hoyle-analog state in $3/2^-$ states, because of the fragmentation of ^{12}C$(0_2^+) \otimes 0p_{3/2}$ configuration into many states. The absence of the Hoyle-analog states in P-wave states is attributed to the strong α-n P-wave interaction. On the hand, the $1/2_2^+$ state located at 15.4 MeV is a Hoyle-analog state dominated by the ^{12}C$(0_2^+) \otimes 1s_{1/2}$ configuration with $S = 0.64$.

The characters of the $1/2^-$ and $1/2^+$ states are reflected to the IS0 and IS1 transitions. The IS0 transitions to the excited $1/2^-$ states are comparable to the Hoyle state in ^{12}C. The origin of the enhanced IS0 transitions is the clustering nature of the excited $1/2^-$ states. In particular, the enhanced $M(IS0)$ of the $1/2_3^-$, $1/2_4^-$, and $1/2_5^-$ originate in the coupling of the ^{12}C$(0_2^+) \otimes 1s_{1/2}$ and ^{12}C$(2_2^+) \otimes 0p_{3/2}$ configurations. In contrast, the IS1 transition to the Hoyle-analog $1/2_2^+$ state is suppressed due to the property of the IS1 transition operator.

The decay widths of the $1/2^+$ states show very unique patterns. The Hoyle-analog $1/2_2^+$ state dominantly decays via the ^{12}C$(0_2^+) \otimes s_{1/2}$ channel but the $1/2_3^+$ state decays via the ^{9}Be$(3/2_1^-) \otimes l = 1$ channel. These unique decay patterns are key observables to identify the Hoyle-analog $1/2^+$ state.

[1] E. Uegaki, S. Okaba, Y. Abe, and H. Tanaka, Prog. Theor. Phys. **57**, 1262 (1977).

[2] M. Kamimura, Nucl. Phys. A **351**, 456 (1981).

[3] Y. Kanada-En'yo, Phys. Rev. Lett. **81**, 5291 (1998).

[4] A. Tohsaki, H. Horiuchi, P. Schuck, and G. Röpke, Phys. Rev. Lett. **87**, 192501 (2001).

[5] Y. Funaki, A. Tohsaki, H. Horiuchi, P. Schuck, and G. Röpke, Phys. Rev. C **67**, 051306(R) (2003).

[6] M. Chernykh, H. Feldmeier, T. Neff, P. von Neumann-Cosel, and A. Richter, Phys. Rev. Lett. **98**, 032501 (2007).

[7] Y. Funaki, T. Yamada, H. Horiuchi, G. Ropke, P. Schuck, and A. Tohsaki, Phys. Rev. Lett. **101**, 082502 (2008).

[8] T. Wakasa et al., Phys. Lett. B **653**, 173 (2007).

[9] N. Curtis et al., Phys. Rev. C **94**, 034313 (2016).

[10] K. C. W. Li, R. Neveling, P. Adsley, P. Papka, F. D. Smit, J. W. Brummer, C. A. Diget, M. Freer, M. N. Harakeh, T. Kokalova, F. Nemulodi, L. Pellegri, B. Rebeiro, J.A. Swartz, S. Triambak, J. J. van Zyl, and C. Wheldon, Phys. Rev. C **95**, 031302(R) (2017).

[11] T. Yamada and P. Schuck, Phys. Rev. C **69**, 024309 (2004).

[12] Y. Kanada-En'yo, Phys. Rev. C **75**, 024302 (2007).

[13] T. Suhara and Y. Kanada-En'yo, Phys. Rev. C **85**, 054320 (2012).

[14] T. Yamada and Y. Funaki, Phys. Rev. C **82**, 064315 (2010).

[15] T. Yamada, H. Horiuchi, and P. Shuck, Mod. Phys. Lett. A **21**, 2373 (2006).

[16] T. Yamada and Y. Funaki, Phys. Rev. C **92**, 034326 (2015).

[17] T. Kawabata et al., Phys. Lett B **646**, 6 (2007).

[18] T. Yamada, Y. Funaki, H. Horiuchi, K. Ikeda, and A. Tohsaki, Prog. Theor. Phys. **120**, 1139 (2008).

[19] T. Yamada, Y. Funaki, T. Myo, H. Horiuchi, K. Ikeda, G. Ropke, P. Schuck, and A. Tohsaki, Phys. Rev. C **85**, 034315 (2012).

[20] Y. Chiba, M. Kimura, and Y. Taniguchi, Phys. Rev. C **93**, 034319 (2016).

[21] M. Kimura, T. Suhara, and Y. Kanada-En'yo, Eur. Phys. J A **52**, 373 (2016).

[22] J. F. Berger, M. Girod, and D. Gogny, Comput. Phys. Commun. **63**, 365 (1991).

[23] Y. Kanada-En'yo, M. Kimura, and H. Horiuchi, C. R. Phys. **4**, 497 (2003).

[24] M. Kimura, Phys. Rev. C **69**, 044319 (2004).

[25] H. Horiuchi, K. Ikeda, and K. Katō, Prog. Theor. Phys. Suppl. **192**, 1 (2012).

[26] Y. Chiba and M. Kimura, Phys. Rev. C **91**, 061302(R) (2015).

[27] Y. Chiba and M. Kimura, Prog. Theor. Exp. Phys. **2017**, 053D01 (2017).

[28] F. Ajzenberg-selove, J. H. Kelley, and C. D. Nesaraja, Nucl. Phys. A **523**, 1 (1991).

[29] T. Kawabata *et al.*, Int. Mod. Phys. E **17**, 2071 (2008).

[30] T. Kawabata *et al.*, in *Nuclear Physics Trends: 7th JapanChina Joint Nuclear Physics Symposium*, edited by A. Ozawa and W. Lu, AIP Conf. Proc. No. 1235 (AIP, New York, 2010). p. 207.

[31] T. Kawabata (private communication).

[32] N. Furutachi and M. Kimura, Phys. Rev. C **83**, 021303(R) (2011).

[33] M. Millin and W. von Oertzen, Eur. Phys. J. A **14**, 295 (2002).

[34] Y. Kanada-En'yo, Prog. Theor. Phys. **117**, 655 (2007).

[35] M. Kimura, Phys. Rev. C **95**, 034331 (2017).